Electronic Research Archive

https://www.aimspress.com/journal/era

ERA, 32(7): 4723–4740.
DOI: 10.3934/era.2024215
Received: 21 May 2024
Revised: 11 July 2024
Accepted: 23 July 2024
Published: 29 July 2024

Research article

Spatiotemporal patterns of a delayed diffusive prey-predator model with prey-taxis

Fengrong Zhang* **and Ruining Chen**

College of Science, China University of Petroleum (East China), Qingdao 266580, China

* **Correspondence:** Email: zhangfengrongsong@126.com.

Abstract: This paper explored a delayed diffusive prey-predator model with prey-taxis involving the volume-filling mechanism subject to homogeneous Neumann boundary condition. To figure out the impact on the dynamic of the prey-predator model due to prey-taxis and time delay, we treated the prey-tactic coefficient χ and time delay τ as the bifurcating parameters and did stability and bifurcation analysis. It showed that the time delay will induce Hopf bifurcations in the absence of prey-taxis, and the bifurcation periodic solution at the first critical value of τ was spatially homogeneous. Hopf bifurcations occurred in the model when the prey-taxis and time delay coexisted, and at the first critical value of τ, spatially homogeneous or nonhomogeneous periodic solutions might emerge. It was also discovered that the bifurcation curves will intersect, which implied that Hopf-Hopf bifurcations can occur. Finally, we did numerical simulations to validate our outcomes.

Keywords: prey-predator model; stability; prey-taxis; delay; nonhomogeneous Hopf bifurcation

1. Introduction

The prey-predator model is a kind of essential differential equation to investigate the intricate relationship between prey and predator. It was suggested by Lotka [1] and Volterra [2], and since then, many mathematicians have studied this problem and many improved models have been formulated. Nowadays, the problem has been a core topic in math and biology, and studying it can help us better understand the nature and dynamics of differential equations.

The prey-predator models represented by ordinary differential equations have been discussed extensively for years, and as time went on and with the development of mathematics, partial differential equations were introduced to describe the spatial effect [3–7]. Besides random diffusion, directed movement should be considered because predators will move toward places where the prey is plentiful. This phenomenon is called chemotaxis. The first chemotaxis model was proposed by Keller and Segel [8, 9], and it attracted many mathematicians' attention [10–12]. The chemotaxis is introduced

in the prey-predator model and there are two types, prey-taxis and predator-taxis. In order to further simulate the real situation and prevent overcrowding, Hillen and Painter et al. described the mechanism of volume effects in [13, 14]. Based on the reasonable choice of $q(v) = 1 - \frac{v}{\gamma}, 0 \le v < \gamma$ [10], Hao et al. [15] investigated the model with volume-filling mechanism,

$$\begin{cases} u_t = d_1\Delta u + u(1-u) - hu - \frac{suv}{\beta+u}, & x \in \Omega, t > 0, \\ v_t = d_2\Delta v - \nabla\cdot(mv\nabla u) + \alpha(\frac{uv}{\beta+u} - \frac{rv^2}{1+rv}), & x \in \Omega, t > 0, \\ \frac{\partial u}{\partial \nu} = \frac{\partial v}{\partial \nu} = 0, & x \in \partial\Omega, t > 0, \\ u(x,0) = u_0(x) \ge 0, v(x,0) = v_0(x) \ge 0, & x \in \Omega, \end{cases} \tag{1.1}$$

where Ω is a bound domain in R^n ($n \ge 1$) with smooth boundary $\partial\Omega$, ν is the unit outward normal vector of $\partial\Omega$, and Δ is the Laplace operator on Ω. u and v represent the densities of prey and predator at location x and time t, respectively, and u_0 and v_0 are assumed to be nonnegative and bound in Ω. $d_1, d_2 > 0$ are the random diffusion coefficients of prey and predator, respectively, and they are independent of time and space, and h is the harvesting coefficient; the effect of harvesting has been discussed in [16]. s, β, α, r are all positive and their exact meanings can be referred to [17]. The chemotaxis term $\nabla\cdot(mv\nabla u)$ denotes the possibility that the predator will travel in the gradient direction of prey, where m stands for the sensitivity, which is defined by

$$m = m(v) = \begin{cases} \chi(1 - \frac{v}{v_p}), & 0 \le v < v_p, \\ 0, & v \ge v_p. \end{cases} \tag{1.2}$$

χ is the chemotaxis coefficient, v_p is the maximum value of the accommodate capacity in a unit volume. From the definition of m, it can be interpreted that if the number of predators exceeds v_p, no predator will move to the unit volume. When $v \ge v_p$, the chemotactic response will be switched off so that the authors in [15] just considered the case $0 \le v < v_p$.

It is well-known that time delay reflects the delay in response time between prey and predator, in the process of predation. There are many phenomena of time delay, for example, predators need time to convert the energy they got from prey to reproduce [18]; newborns becoming adults also need time [19]; and species spend time moving between two areas [20, 21]. In contrast to the model without time delay, the delayed equations are more realistic and may induce more complex dynamics [22]. Shi and Song studied a model that combines both prey-taxis and time delay [23], which shows that the combined influence of prey-taxis and time delay will induce interesting and different dynamics.

Motivated by the above research, assuming that the predation in the earlier times will decrease the rate of the prey population in later times [24], we incorporate a time delay into the system (1.1) and take $\Omega = (0, l\pi)$, then system (1.1) becomes the following system:

$$\begin{cases} u_t = d_1u_{xx} + u(1-u) - hu - \frac{suv_\tau}{\beta+u}, & x \in (0,l\pi), t > 0, \\ v_t = d_2v_{xx} - (mvu_x)_x + \alpha(\frac{uv}{\beta+u} - \frac{rv^2}{1+rv}), & x \in (0,l\pi), t > 0, \\ u_x(0,t) = u_x(l\pi,t) = 0, v_x(0,t) = v_x(l\pi,t) = 0, & t > 0, \\ u(x,t) = u_0(x,t) \ge 0, v(x,t) = v_0(x,t) \ge 0, & x \in [0,l\pi], t \in [-\tau, 0], \end{cases} \tag{1.3}$$

where $v_\tau = v(x, t-\tau)$, and τ denotes the time delay.

In the absence of time delay and volume-filling mechanism, the system (1.3) has been studied in [16]. Hao et al. studied the model with only prey-taxis with the volume-filling mechanism in [15],

and they proved that the prey-taxis with the volume-filling mechanism will induce steady state bifurcation, but it has no impact on the appearance of Hopf bifurcation. In the present paper, we mainly concentrate on the combined effect of time delay and prey-taxis involving volume-filling mechanism on the dynamics of the system (1.3), so we just consider the case $0 \le v < v_p$, which indicates $m(v) > 0$.

The framework of this paper is as follows. Section 2 mainly discusses the cases $\chi = 0, \tau > 0$ and $\chi > 0, \tau > 0$. By solving the characteristic equation and treating χ and τ as bifurcating parameters, we obtain the stability and bifurcation results. The results of numerical simulations are displayed in Section 3. Section 4 shows the conclusion of this paper. Throughout the paper, $\mathbb{N}$ denotes the set of positive integers and $\mathbb{N}_0 = \mathbb{N} \cup 0$.

2. Stability and Hopf bifurcations

To begin, we explore the stability of the system (1.3) with $\chi = 0, \tau > 0$ and $\chi > 0, \tau > 0$, respectively. By direct calculation, the system (1.3) has three equilibria: (0,0), $(1-h, 0)$ $(0 < h < 1)$, and the unique positive constant equilibrium (u_*, v_*), where

$$u_* = \frac{(1-\beta-h-\frac{s}{\beta r})+\sqrt{(1-\beta-h-\frac{s}{\beta r})^2+4\beta(1-h)}}{2}, \quad v_* = \frac{u_*}{\beta r}. \tag{2.1}$$

It is apparent to infer that the equilibria $(0, 0)$ and $(1-h, 0)$ are unstable. Then, we consider the stability of (u_*, v_*).

Linearizing the system (1.3) at (u_*, v_*), we have

$$\begin{pmatrix} u_t \\ v_t \end{pmatrix} = \begin{pmatrix} d_1\Delta & 0 \\ -m_* v_* \Delta & d_2\Delta \end{pmatrix}\begin{pmatrix} u \\ v \end{pmatrix} + \begin{pmatrix} 1-2u_*-h-\frac{sv_*\beta}{(\beta+u_*)^2} & 0 \\ \frac{\alpha\beta v_*}{(\beta+u_*)^2} & -\frac{\alpha r v_*}{(1+rv_*)^2} \end{pmatrix}\begin{pmatrix} u \\ v \end{pmatrix} + \begin{pmatrix} 0 & -\frac{su_*}{\beta+u_*} \\ 0 & 0 \end{pmatrix}\begin{pmatrix} u_\tau \\ v_\tau \end{pmatrix}. \tag{2.2}$$

Since u_* satisfies $u_*(1-u_*) - hu_* - \frac{su_*v_*}{\beta+u_*} = 0, u_* \neq 0$, we can obtain

$$1-2u_*-h-\frac{sv_*\beta}{(\beta+u_*)^2} = u_*(\frac{sv_*}{(\beta+u_*)^2} - 1),$$

and

$$\frac{\alpha r v_*}{(1+rv_*)^2} = \frac{\alpha\beta u_*}{(\beta+u_*)^2},$$

because of $v_* = \frac{u_*}{\beta r}$.

For convenience, let

$$\begin{aligned} &\theta = u_*(1-\frac{sv_*}{(\beta+u_*)^2}), && \eta = \frac{\alpha\beta u_*}{(\beta+u_*)^2}, \\ &\delta = \frac{su_*}{\beta+u_*} > 0, && \rho = (1-\frac{v_*}{v_p})v_* > 0, \end{aligned} \tag{2.3}$$

then linearized system (2.2) can be rewritten as

$$\begin{pmatrix} u_t \\ v_t \end{pmatrix} = \begin{pmatrix} d_1\Delta & 0 \\ -\chi\rho\Delta & d_2\Delta \end{pmatrix}\begin{pmatrix} u \\ v \end{pmatrix} + \begin{pmatrix} -\theta & 0 \\ \frac{\eta}{\beta r} & -\eta \end{pmatrix}\begin{pmatrix} u \\ v \end{pmatrix} + \begin{pmatrix} 0 & -\delta \\ 0 & 0 \end{pmatrix}\begin{pmatrix} u_\tau \\ v_\tau \end{pmatrix}. \tag{2.4}$$

When $\chi = 0, \tau = 0$, we know from [22] that the positive constant equilibrium (u_*, v_*) is locally asymptotically stable if

$$\theta \geq 0, \quad 0 < h < 1. \tag{2.5}$$

Our analysis in the following paper is based on condition (2.5). When $\chi > 0, \tau = 0$, the conclusions in [15] reveal that χ can't induce Turing and Hopf bifurcations for $\theta \geq 0$. Next, we consider the other two cases.

When $\chi = 0, \tau > 0$, the linearized system (2.4) turns to

$$\begin{pmatrix} u_t \\ v_t \end{pmatrix} = \begin{pmatrix} d_1\Delta & 0 \\ 0 & d_2\Delta \end{pmatrix} \begin{pmatrix} u \\ v \end{pmatrix} + \begin{pmatrix} -\theta & 0 \\ \frac{\eta}{\beta r} & -\eta \end{pmatrix} \begin{pmatrix} u \\ v \end{pmatrix} + \begin{pmatrix} 0 & -\delta \\ 0 & 0 \end{pmatrix} \begin{pmatrix} u_\tau \\ v_\tau \end{pmatrix}.$$

Then, the corresponding characteristic equation is

$$\lambda^2 + (d_1\mu_k + d_2\mu_k + \theta + \eta)\lambda + (d_1\mu_k + \theta)(d_2\mu_k + \eta) + \frac{\eta\delta}{\beta r}e^{-\lambda\tau} = 0, \tag{2.6}$$

where μ_k is the eigenvalues of $-\Delta$ in $\Omega = (0, l\pi)$ under the homogeneous Neumann boundary condition, and $0 = \mu_0 < \mu_1 < \mu_2 < \cdots < \mu_k = \frac{k^2}{l^2} < \cdots$. Coincidentally, Eq (2.6) is the same as the characteristic equation in [22], where the reader can refer to it for more details and concrete content.

When $\chi > 0, \tau > 0$, the characteristic equation of linearized system (2.4) can be written as

$$\lambda^2 + (d_1\mu_k + \theta + d_2\mu_k + \eta)\lambda + (d_1\mu_k + \theta)(d_2\mu_k + \eta) + \delta(\chi\rho\mu_k + \frac{\eta}{\beta r})e^{-\lambda\tau} = 0. \tag{2.7}$$

Specifically, when $\theta \geq 0$, all the conditions of Theorem 2.2 in [15] are satisfied, which implies that all the roots of Eq (2.7) with $\tau = 0$ have negative real parts. For $\tau > 0$, substituting $\lambda = 0$ into Eq (2.7), we can see that

$$(d_1\mu_k + \theta)(d_2\mu_k + \eta) + \delta(\chi\rho\mu_k + \frac{\eta}{\beta r}) = 0, \tag{2.8}$$

and it is obvious that no $\mu_k > 0$ satisfies Eq (2.8) due to the positivity of all the coefficients of Eq (2.8), which indicates that the steady state bifurcation will not emerge in the system (1.3).

Next, we mainly study the Hopf bifurcation. As we all know, the necessary condition for Hopf bifurcation to occur is Eq (2.7) has purely imaginary roots $\pm i\omega_k$ ($\omega_k > 0$). Substituting $\lambda = i\omega_k$ into Eq (2.7), we can obtain

$$-\omega_k^2 + (d_1\mu_k + d_2\mu_k + \theta + \eta)i\omega_k + (d_1\mu_k + \theta)(d_2\mu_k + \eta) + \delta(\chi\rho\mu_k + \frac{\eta}{\beta r})e^{-i\omega_k\tau} = 0. \tag{2.9}$$

Separating the real and imaginary parts of Eq (2.9), we conclude that

$$\begin{cases} \cos(\omega_k\tau) &= \dfrac{\omega_k^2 - (d_1\mu_k + \theta)(d_2\mu_k + \eta)}{\delta(\chi\rho\mu_k + \frac{\eta}{\beta r})}, \\ \sin(\omega_k\tau) &= \dfrac{(d_1\mu_k + \theta + d_2\mu_k + \eta)\omega_k}{\delta(\chi\rho\mu_k + \frac{\eta}{\beta r})}, \end{cases} \tag{2.10}$$

thus we have

$$\omega_k^4 + ((d_1\mu_k + \theta)^2 + (d_2\mu_k + \eta)^2)\omega_k^2 + (d_1\mu_k + \theta)^2(d_2\mu_k + \eta)^2 - \delta^2(\chi\rho\mu_k + \frac{\eta}{\beta r})^2 = 0. \tag{2.11}$$

It is clear that $(d_1\mu_k + \theta)^2 + (d_2\mu_k + \eta)^2 > 0$ holds, and we can infer that Eq (2.11) has positive roots only if

$$(d_1\mu_k + \theta)^2(d_2\mu_k + \eta)^2 - \delta^2(\chi\rho\mu_k + \frac{\eta}{\beta r})^2 < 0,$$

which implies

$$(d_1\mu_k + \theta)(d_2\mu_k + \eta) - \delta(\chi\rho\mu_k + \frac{\eta}{\beta r}) < 0. \tag{2.12}$$

Subsequently, we determine the range for μ_k satisfying Eq (2.12).

Lemma 2.1. *Let $\theta, \eta, \delta, \rho$ be defined in Eq (2.3), and θ, h satisfy Eq (2.5). Define:*

$$\chi_2 = \frac{1}{\delta\rho}(d_1\eta + d_2\theta + 2\sqrt{d_1d_2\eta(\theta - \frac{\delta}{\beta r})}), \tag{2.13}$$

$$y_-(\chi) = \frac{1}{2d_1d_2}(-(d_1\eta + d_2\theta - \chi\rho\delta) - \sqrt{(d_1\eta + d_2\theta - \chi\rho\delta)^2 - 4d_1d_2\eta(\theta - \frac{\delta}{\beta r})}), \tag{2.14}$$

$$y_+(\chi) = \frac{1}{2d_1d_2}(-(d_1\eta + d_2\theta - \chi\rho\delta) + \sqrt{(d_1\eta + d_2\theta - \chi\rho\delta)^2 - 4d_1d_2\eta(\theta - \frac{\delta}{\beta r})}). \tag{2.15}$$

(I) if $\theta < \frac{\delta}{\beta r}$, Eq (2.12) holds when $0 \le \mu_k < y_+(\chi)$;
(II) if $\theta \ge \frac{\delta}{\beta r}$ and $\chi > \chi_2$, Eq (2.12) holds when $y_-(\chi) < \mu_k < y_+(\chi)$.

Proof. To start, the distribution of the roots of the corresponding quadratic equation of Eq (2.12) will be obtained by letting $y = \mu_k$:

$$d_1d_2y^2 + (d_1\eta + d_2\theta - \delta\chi\rho)y + \theta\eta - \frac{\delta\eta}{\beta r} = 0. \tag{2.16}$$

If $\theta < \frac{\delta}{\beta r}$, it's evident that $y_+(\chi)$ defined in Eq (2.15) is the only positive root of Eq (2.16), and we obtain that Eq (2.12) holds when $0 \le \mu_k < y_+(\chi)$.

If $\theta \ge \frac{\delta}{\beta r}$, we study the discriminant Δ_1 of Eq (2.16):

$$\Delta_1 = (d_1\eta + d_2\theta - \rho\delta\chi)^2 - 4d_1d_2(\theta\eta - \frac{\delta\eta}{\beta r}),$$

when $\Delta_1 > 0$, Eq (2.16) has two roots. By directly calculating, we have $\Delta_1 > 0$ when $\chi < \chi_1 = \frac{1}{\delta\rho}(d_1\eta + d_2\theta - 2\sqrt{d_1d_2\eta(\theta - \frac{\delta}{\beta r})}$ or $\chi > \chi_2 = \frac{1}{\delta\rho}(d_1\eta + d_2\theta + 2\sqrt{d_1d_2\eta(\theta - \frac{\delta}{\beta r})}$. Specifically, Eq (2.16) has no positive roots for $\chi < \chi_1$; however, if $\chi > \chi_2$, Eq (2.16) has two positive roots $y_-(\chi) \ge 0$ and $y_+(\chi) > 0$, which are defined by ((2.14) and (2.15)). Thus, Eq (2.12) holds when $y_-(\chi) < y < y_+(\chi)$.

Based on Lemma 2.1, we will derive the conditions that Eq (2.7) have purely imaginary roots.

Lemma 2.2. *Let $\theta, \eta, \delta, \rho$ be defined in (2.3), $\chi_2, y_-(\chi), y_+(\chi)$ are defined in (2.13)–(2.15), respectively, and θ and h satisfy (2.5). Define:*

$$\underline{\chi} = \begin{cases} \frac{1}{\delta\rho}(\frac{d_1d_2}{l^2} + d_1\eta + d_2\theta + l^2\eta(\theta - \frac{\delta}{\beta r}), & 0 < l \le l_0, \\ 0, & l > l_0, \end{cases} \tag{2.17}$$

$$\hat{\chi} = \min\left\{\chi : [l\sqrt{y_+(\chi)}] - [l\sqrt{y_-(\chi)}] = 1\right\}, \tag{2.18}$$

where

$$l_0 = \sqrt{\frac{d_1\eta + d_2\theta + \sqrt{(d_1\eta + d_2\theta)^2 - 4d_1d_2\eta(\theta - \frac{\delta}{\beta r})}}{-2\eta(\theta - \frac{\delta}{\beta r})}}, \tag{2.19}$$

and $[\cdot]$ *is the integer part function,*

$$\tau_{0j} = \frac{1}{\omega_0}(\arccos\frac{(\omega_0^2 - \theta\eta)\beta r}{\delta\eta} + 2j\pi), \quad (j \in \mathbb{N}_0), \tag{2.20}$$

$$\tau_{kj} = \frac{1}{\omega_k}(\arccos\frac{\omega_k^2 - (d_1\mu_k + \theta)(d_2\mu_k + \eta)}{\delta(\chi\rho\mu_k + \frac{\eta}{\beta r})} + 2j\pi), \tag{2.21}$$

where $0 \le k \le K,\ K = [l\sqrt{y_+(\chi)}],\ j \in \mathbb{N}_0$,

(I) if $\theta < \frac{\delta}{\beta r}$,

(i) if further $0 < \chi \le \underline{\chi}$, *Eq (2.7) has only a pair of purely imaginary roots* $\pm i\omega_0$ *when* $\tau = \tau_{0j}$ *defined in (2.20);*

(ii) if further $\chi > \underline{\chi}$, *Eq (2.7) has pairs of purely imaginary roots* $\pm i\omega_k$ *when* $\tau = \tau_{kj}$ *defined by (2.21);*

(II) if $\theta \ge \frac{\delta}{\beta r}$, *for given* $l > 0$,

(i) if $0 < \chi < \hat{\chi}$, *Eq (2.7) has no imaginary roots for any time delay* $\tau > 0$;

(ii) if $\chi \ge \hat{\chi}$, *Eq (2.7) has pairs of purely imaginary roots* $\pm i\omega_k$ *when* $\tau = \tau_{kj}$ *defined by (2.21), where* $\underline{k} \le k \le K,\ \underline{k} = [l\sqrt{y_-(\chi)}] + 1,\ K = [l\sqrt{y_+(\chi)}],\ j \in \mathbb{N}_0$.

Proof. (I) It is well-known that Eq (2.7) has purely imaginary roots for $k \ge 1$, and there must be at least one μ_k for $k \ge 1$ satisfying Eq (2.12). We know from Lemma 2.1 that $y_+(\chi)$ is the unique positive root of Eq (2.16) if $\theta < \frac{\delta}{\beta r}$. It is obvious from the monotonicity of μ_k that if $\mu_1 \ge y_+(\chi)$, then all other μ_k will not satisfy Eq (2.12), which shows that Eq (2.7) has no purely imaginary roots. Obviously, $y_+(\chi)$ is an increasing function with respect to χ, and $y_+(0)$ is the minimum value of $y_+(\chi)$, then we can solve the critical value l_0 by solving $\mu_1|_{l=l_0} = y_+(0)$, l_0 is defined in (2.19). When $l > l_0$, there must be at least $\mu_1 < y_+(\chi)$ for all $\chi > 0$. Now, we denote $\underline{\chi}$ as the critical value for Eq (2.11) to have positive roots for $k \ge 1$. Then, we have $\underline{\chi} = 0$ when $l > l_0$. When $0 < l \le l_0$, Eq (2.11) has no positive roots for $k \ge 1$ and $0 < \chi \le \underline{\chi}$, where $\underline{\chi}$ is solved by $y_+(\underline{\chi}) = \frac{1}{l^2}$. When $\chi > \underline{\chi}$, it exists some μ_k to satisfy Eq (2.12) because $\mu_1 = y_+(\underline{\chi}) < y_+(\chi)$. Next, the number of the roots of Eq (2.11) can be determined by calculating $\frac{K^2}{l^2} < y_+(\chi)$ and have $K = [l\sqrt{y_+(\chi)}]$. Therefore, from (2.10), we derive Eq (2.7) has purely imaginary roots $\pm i\omega_k$ at τ_{kj} defined by Eq (2.21) for $0 \le k \le K$ and $j \in \mathbb{N}_0$.

(II) If $\theta \ge \frac{\delta}{\beta r}$ and $0 < \chi \le \chi_2$, it's obvious from the proof of Lemma 2.1 that Eq (2.12) has no positive roots. Nevertheless, if $\chi > \chi_2$, we know that Eq (2.12) holds for $y_-(\chi) < \mu_k < y_+(\chi)$. Then, for given $l > 0$, the number of the roots of Eq (2.11) can be calculated by solving $y_-(\chi) < \frac{k^2}{l^2} < y_+(\chi)$ and we obtain $l\sqrt{y_-(\chi)} < k < l\sqrt{y_+(\chi)}$. Let $\psi(\chi) = [l\sqrt{y_+(\chi)}] - [l\sqrt{y_-(\chi)}]$, where $[\cdot]$ is the integer part function. It is clear that $\psi(\chi)$ is an increasing piecewise function and $\psi(\chi_2) = 0$, so, for given $l > 0$, it is impossible that Eq (2.11) has positive roots for $k \ge 1$ and $\chi_2 < \chi < \hat{\chi}$ with $\hat{\chi}$ as in (2.18). When

$\chi \geq \hat{\chi}$, there must exist some $\mu_k,\ k \geq 1$ that Eq (2.11) has positive roots for given $l > 0$. Furthermore, the value of the roots of Eq (2.11) can be solved by letting $\mu_{\underline{k}} > y_-(\chi)$ and $\mu_K < y_+(\chi)$, and we obtain $\underline{k} = [l\sqrt{y_-(\chi)}] + 1$ and $K = [l\sqrt{y_+(\chi)}]$. Then, we similarly solve from Eq (2.10) that Eq (2.7) has purely imaginary roots $\pm i\omega_k$ at τ_{kj} for $\underline{k} \leq k \leq K$ and $j \in \mathbb{N}_0$, where τ_{kj} is defined by (2.21).

So, the proof is finished.

Lemma 2.3. *Let $\theta, \eta, \delta, \rho$ be defined in (2.3), and θ, h satisfy (2.5). If $\theta < \frac{\delta}{\beta r}$ and $j = 0$, Eqs (2.20) and (2.21) can be rewritten as*

$$\begin{cases} \tau_{00} = \dfrac{1}{\omega_0} \arccos \dfrac{(\omega_0^2 - \theta\eta)\beta r}{\delta\eta} \\ \tau_{k0}(\chi) = \dfrac{1}{\omega_k(\chi)} \arccos \dfrac{\omega_k(\chi)^2 - (d_1\mu_k + \theta)(d_2\mu_k + \eta)}{\delta(\chi\rho\mu_k + \frac{\eta}{\beta r})}, \ 1 \leq k \leq K, \end{cases} \tag{2.22}$$

where K is the same as in Lemma 2.2. We have the following conclusions,

(I) τ_{00} is a constant, $\tau_{k0}(\chi)$ $(1 \leq k \leq K)$ is decreasing as χ increases; moreover, we have $\lim\limits_{\chi \to +\infty} \tau_{k0}(\chi) = 0$;

(II) $\tau_{k0}(0)$ $(0 \leq k \leq K)$ is monotonically increasing with respect to k, i.e., $\tau_{00}(0) < \tau_{10}(0) < \cdots < \tau_{K0}(0)$.

Proof. (I) It's obviously that τ_{00} is a constant. When $1 \leq k \leq K$, taking derivative of $\tau_{k0}(\chi)$ in χ, we have

$$\frac{d(\tau_{k0}(\chi))}{d\chi} = -\frac{2\omega_k\omega_k'(\chi)(\chi\rho\mu_k + \frac{\eta}{\beta r}) - \rho\mu_k(\omega_k^2 - (d_1\mu_k + \eta)(d_2\mu_k + \theta))}{\omega_k\delta(\chi\rho\mu_k + \frac{\eta}{\beta r})^2\sqrt{1 - R_k^2}} - \frac{\omega_k'(\chi)\arccos R_k}{\omega_k^2}, \tag{2.23}$$

where

$$R_k = \frac{\omega_k^2 - (d_1\mu_k + \theta)(d_2\mu_k + \eta)}{\delta(\chi\rho\mu_k + \frac{\eta}{\beta r})}.$$

Differentiating both sides of Eq (2.11) with respect to χ, we gain

$$\omega_k'(\chi) = \frac{\delta^2\rho\mu_k(\rho\mu_k\chi + \frac{\eta}{\beta r})}{2\omega_k(\chi)^3 + \omega_k(\chi)((d_1\mu_k + \theta)^2 + (d_2\mu_k + \eta)^2)} > 0,$$

then substituting $\omega_k'(\chi)$ into Eq (2.23), we have

$$\frac{d(\tau_{k0}(\chi))}{d\chi} = -\frac{\rho\mu_k(d_1\mu_k + \theta + d_2\mu_k + \eta)^2(\omega_k^2 + (d_1\mu_k + \theta)(d_2\mu_k + \eta))}{\omega_k\delta(\chi\rho\mu_k + \frac{\eta}{\beta r})^2\sqrt{1 - R_k^2}(2\omega_k^2 + (d_1\mu_k + \theta)^2(d_2\mu_k + \eta)^2)} - \frac{\omega_k'(\chi)\arccos R_k}{\omega_k^2}. \tag{2.24}$$

It can be found that $0 < \arccos R_k < \pi$; therefore, $\frac{d(\tau_{k0}(\chi))}{d\chi} < 0$, that is to say, τ_{k0} is decreasing as χ increases. Clearly, we can see that $\omega_k \to +\infty$ when $\chi \to +\infty$, so it's established $\lim\limits_{\chi \to +\infty} \tau_{k0} = \lim\limits_{\chi \to +\infty} \frac{\arccos R_k}{\omega_k} = 0$.

(II) When $\chi = 0$, denoting $\mu_k = p$, then $\tau_{k0}(0)$ $(0 \le k \le K)$ and $\omega_k(0)$ can be seen as a function $\tilde{\tau}_{k0}(p)$ and $\tilde{\omega}_k(p)$, respectively, of p. Obviously, $\tilde{\omega}_k(p)$ satisfies

$$\tilde{\omega}_k(p)^4 + ((d_1p+\theta)^2 + (d_2p+\eta)^2)\tilde{\omega}_k(p)^2 + (d_1p+\theta)^2(d_2p+\eta)^2 = \delta^2(\frac{\eta}{\beta r})^2, \tag{2.25}$$

and

$$\tilde{\tau}_{k0}(p) = \frac{1}{\tilde{\omega}_k(p)} \arccos \tilde{R}(p),$$

where

$$\tilde{R}(p) = \frac{\tilde{\omega}_k(p)^2 - (d_1p+\theta)(d_2p+\eta)}{\delta\eta/\beta r}.$$

Differentiating at both sides of Eq (2.25) with respect to p, we have

$$\tilde{\omega}_k'(p) = -\frac{\tilde{\omega}_k^2(p)(d_1(d_1p+\theta)+d_2(d_2p+\eta)) + d_1(d_1p+\theta)(d_2p+\eta)^2 + d_2(d_1p+\theta)^2(d_2p+\eta)}{2\tilde{\omega}_k^3(p) + \tilde{\omega}_k(p)((d_1p+\theta)^2 + (d_2p+\eta)^2)} < 0. \tag{2.26}$$

We take derivative of $\tilde{\tau}_{k0}(p)$ with respect to p, and we get

$$\frac{d(\tilde{\tau}_{k0}(p))}{dp} = -\frac{\beta r(2\tilde{\omega}_k(p)\tilde{\omega}_k'(p) - d_1(d_1p+\theta) + d_2(d_2p+\eta))}{\rho\delta\tilde{\omega}_k(p)\sqrt{1-\tilde{R}(p)^2}} - \frac{\tilde{\omega}_k'(p)\arccos\tilde{R}(p)}{\tilde{\omega}_k^2(p)} > 0. \tag{2.27}$$

From Eq (2.27), we find that $\tilde{\tau}_{k0}(p)$ is monotonically increasing with respect to p. Thus, $\tau_{k0}(0)$ is increasing with respect to k, that is, $\tau_{00}(0) < \tau_{10}(0) < \cdots < \tau_{K0}(0)$.

Afterward, we verify the transversality condition of Hopf bifurcation.

Lemma 2.4. *Let $\theta, \eta, \rho, \delta$ be defined in (2.3), and θ, h satisfy (2.5). We have*

$$\left.\frac{dRe(\lambda)}{d\tau}\right|_{\tau=\tau_{kj}} > 0.$$

Proof. To begin, we take the derivative at both sides of Eq (2.7) with respect to τ and obtain

$$2\lambda\lambda'(\tau) + (d_1\mu_k + d_2\mu_k + \theta + \eta)\lambda'(\tau) - \delta(\chi\rho\mu_k + \frac{\eta}{\beta r})(\lambda'(\tau)\tau + \lambda)e^{-\lambda\tau} = 0,$$

therefore,

$$\lambda'(\tau) = \frac{\lambda\delta(\chi\rho\mu_k + \frac{\eta}{\beta r})e^{-\lambda\tau}}{2\lambda + (d_1\mu_k + d_2\mu_k + \theta + \eta) - \tau\delta(\chi\rho\mu_k + \frac{\eta}{\beta r})e^{-\lambda\tau}}, \tag{2.28}$$

and (2.28) is equivalent to

$$\frac{1}{\lambda'(\tau)} = \frac{(2\lambda + d_1\mu_k + d_2\mu_k + \theta + \eta)e^{\lambda\tau}}{\lambda\delta(\chi\rho\mu_k + \frac{\eta}{\beta r})} - \frac{\tau}{\lambda}. \tag{2.29}$$

Substituting $\lambda = i\omega_k$ and $\tau = \tau_{kj}$ into the Eq (2.29), we have

$$Re(\frac{1}{\lambda'(\tau)})\Big|_{\tau=\tau_{kj}} = \frac{2\omega_k\cos(\omega_k\tau_{kj}) + \sin(\omega_k\tau_{kj})(d_1\mu_k + d_2\mu_k + \theta + \eta)}{\omega_k\delta(\chi\rho\mu_k + \frac{\eta}{\beta r})}, \tag{2.30}$$

and from Eq (2.10), we can obtain

$$Re(\frac{1}{\lambda'(\tau)})\Big|_{\tau=\tau_{kj}} = \frac{2\omega_k(\omega_k^2 - (d_1\mu_k + \theta)(d_2\mu_k + \eta)) + \omega_k(d_1\mu_k + d_2\mu_k + \theta + \eta)^2}{\omega_k\delta^2(\chi\rho\mu_k + \frac{\eta}{\beta r})^2} > 0. \tag{2.31}$$

Thus, $\frac{dRe(\lambda)}{d\tau}\Big|_{\tau=\tau_{kj}} > 0$, and the proof is completed.

Combining the Lemmas 2.2–2.4, we obtain important results on the stability and Hopf bifurcation as follows.

Theorem 2.1. *Let $\theta, \eta, \delta, \rho$ be defined in (2.3), $y_+(\chi), \underline{\chi}, \tau_{kj}$ be defined in (2.15), (2.17), (2.21), and θ, h satisfy (2.5). Denote*

$$\bar{\chi} = \min_{1\le k\le K}\chi_k,\ \chi_k \text{ is the solution of } \tau_{00} = \tau_{k0}(\chi), \tag{2.32}$$

$$\underline{\tau} = \min_{1\le k\le K}\tau_{k0}(\chi),\ \ \chi > \bar{\chi}. \tag{2.33}$$

If $\theta < \frac{\delta}{\beta r}$, we have results as follows:

(I) (Bifurcation)

- *(i) if $0 < \chi \le \underline{\chi}$, system (1.3) undergoes Hopf bifurcations at $\tau = \tau_{0j}$ for $j \in N_0$ and $\tau_{00} = \min_{j\in N_0}\tau_{0j}$ is the first critical bifurcation value. Moreover, the bifurcating periodic solutions at τ_{00} are spatially homogeneous;*
- *(ii) if $\underline{\chi} < \chi \le \bar{\chi}$, system (1.3) undergoes mode-k Hopf bifurcations at $\tau = \tau_{kj}$ for $0 \le k \le K$, $j \in N_0$. Similarly, $\tau_{00} = \min_{0\le k\le K}\tau_{k0}$, so the bifurcating periodic solutions at τ_{00} are also spatially homogeneous;*
- *(iii) if $\chi > \bar{\chi}$, system (1.3) undergoes mode-k Hopf bifurcations at $\tau = \tau_{kj}$ for $0 \le k \le K$, $j \in N_0$. Furthermore, the first Hopf bifurcation at $\underline{\tau}$ defined by (2.33) is spatially nonhomogeneous;*
- *(iv) if $\chi > \underline{\chi}$, Hopf-Hopf bifurcation will occur because of the interaction of spatially homogeneous and nonhomogeneous Hopf bifurcations;*

(II) (stability)

- *(i) if $0 < \chi \le \bar{\chi}$, (u_*, v_*) is locally asymptotically stable for $0 \le \tau < \tau_{00}$ and unstable for $\tau > \tau_{00}$;*
- *(ii) if $\chi > \bar{\chi}$, (u_*, v_*) is locally asymptotically stable for $0 \le \tau < \underline{\tau}$ and unstable for $\tau > \underline{\tau}$.*

Proof. From Lemmas 2.2–2.4, the necessary conditions for Hopf bifurcation to occur, i.e., the characteristic equation of system (1.3) has purely imaginary roots, the transversality condition of Hopf bifurcation is satisfied, thus system (1.3) indeed undergoes Hopf bifurcation at $\tau = \tau_{kj}$. It's easy to know $\tau_{k0} = \min_{j\in\mathbb{N}_0}\tau_{kj}$ $(0 \le k \le K)$.

If $0 < \chi \le \underline{\chi}$, Eq (2.7) exists only a pair of purely imaginary roots when $\tau = \tau_{0j}$ $(j \in \mathbb{N}_0)$, which implies only spatially homogeneous Hopf bifurcation will emerge. The proof of (i) in (I) is finished.

If $\underline{\chi} < \chi \le \bar{\chi}$, we know from Lemmas 2.2 and 2.4 that τ_{kj} $(0 \le k \le K)$ are the Hopf bifurcation values. From Lemma 2.3, $\tau_{k0}(\chi)$ is decreasing in χ and $\lim_{\chi\to\infty}\tau_{k0}(\chi) = 0$, together with $\tau_{k0}(0) > \tau_{00}$ and τ_{00} is a constant, so τ_{k0} and τ_{00} must intersect at χ_k. We can define $\bar{\chi}$ as in (2.32), thus $\tau_{00} = \min_{0\le k\le K}\tau_{k0}(\chi)$ for $\chi < \bar{\chi}$. The proof of (ii) in (I) is finished.

When $\chi > \bar{\chi}$, τ_{kj} are still Hopf bifurcation values, and $\tau_{k0} = \min\limits_{j\in\mathbb{N}_0} \tau_{kj}$ from Lemmas 2.2 and 2.4, but the minimal critical value of τ_{k0} will modify as χ changes, thus we define $\underline{\tau}$ in (2.33) as the minimal value. This finishes the proof of (iii) in (I).

It is well-known that τ_{kj} is a function with the variable χ, and τ_{00} is a constant in regard to χ so that τ_{00} is a line parallel to the $\chi-$ axis in the $\tau - \chi$ plane. However, τ_{k0} decreases as χ increases and tends to 0, $\tau_{k0}(0) > \tau_{00}$ $(1 \le k \le K)$, thus the spatially nonhomogeneous Hopf bifurcation curves $\tau = \tau_{k0}(\chi)$ will interact with spatial homogeneous Hopf bifurcation curve τ_{00}, so conclusion (iv) in (I) is proved.

It's easy to obtain the stability results (II) from the bifurcation conclusions in (I).

Similarly, we have the stability and Hopf bifurcation results when $\theta \ge \frac{\delta}{\beta r}$ as follows.

Theorem 2.2. *Let $\theta, \eta, \delta, \rho$ be defined in (2.3), θ, h satisfy (2.5), and $\hat{\chi}, \tau_{kj}$ are defined in (2.18) and (2.21), respectively. Let*

$$\tau_* = \min_{\underline{k}\le k\le K} \tau_{k0}(\chi),\ \chi \ge \hat{\chi}. \tag{2.34}$$

If $\theta \ge \frac{\delta}{\beta r}$, we have the results as follows.

(I) if $0 < \chi < \hat{\chi}$, system (1.3) has no Hopf bifurcation for any $\tau > 0$, so (u_*, v_*) is locally asymptotically stable for $\tau > 0$;

(II) if $\chi \ge \hat{\chi}$, system (1.3) undergoes spatially nonhomogeneous mode-k Hopf bifurcations near the positive equilibrium (u_*, v_*) at $\tau = \tau_{kj}$ for $\underline{k} \le k \le K$, $j \in N_0$. Moreover, τ_* defined by (2.34) is the first critical value for Hopf bifurcation, so (u_*, v_*) is locally asymptotically stable for $0 \le \tau < \tau_*$, and unstable for $\tau > \tau_*$.

The proof is analogous to Theorem 2.1, so we leave it out.

Remark 1. According to Theorem 2.1, it is demonstrated that $\underline{\chi}$ just affects the appearance of spatially nonhomogeneous Hopf bifurcation but has no effect on stability when $\theta < \frac{\delta}{\beta r}$. In addition, it is impossible from Theorem 2.2 that the spatially homogeneous Hopf bifurcation will occur for $\theta \ge \frac{\delta}{\beta r}$.

3. Numerical simulation

In this section, we will select appropriate parameters and use the mathematical software Matlab to do numerical simulations for system (1.3), which will support our theoretical results.

3.1. Case I $0 \le \theta < \frac{\delta}{\beta r}$

Taking the parameters as

$$d_1 = 0.01, d_2 = 0.02, r = 1, h = 0.2, s = 1, \alpha = 2, \beta = 0.5, v_p = 1, \tag{3.1}$$

then we have the positive equilibrium $(u_*, v_*) = (0.2095, 0.4190)$, $l_0 = 0.1809, \delta = 0.2953, \theta = 0.0351 < \frac{\delta}{\beta r} = 0.5905$, that is to say, the conditions in Theorem 2.1 are satisfied. It can be found from Lemma 2.2 that $\underline{\chi}$ is a function about l when $l \le l_0$ and $\underline{\chi} = 0$ when $l > l_0$. Only when $\chi > \underline{\chi}$ will the spatial nonhomogeneous Hopf bifurcations will occur, thus we choose $l = 0.1 < l_0$ and $l = 1 > l_0$

to draw the Hopf bifurcation curves diagrams and stable region in the $\chi - \tau$ plane. The results are shown in Figure 1. When $l = 0.1 < l_0$, we have $\underline{\chi} = 0.1698$ and $\bar{\chi} = 0.2843$. Figure 1(a) displays that the spatially nonhomogeneous Hopf bifurcation will emerge for $\chi > \underline{\chi}$. When $l = 1 > l_0$, Figure 1(b) displays that the spatial nonhomogeneous Hopf bifurcations will emerge for $\chi > \underline{\chi} = 0$, and we calculate $\bar{\chi} = 0.1751$. From Figure 1(b), we can see that the Hopf bifurcation curves will intersect with each other, hence Hopf-Hopf bifurcation will occur at the intersecting points. Then, we take some points in different areas of Figure 1(b) to do numerical simulations with the initial values $(u_0, v_0) = (u_* + 0.0004\cos x, v_* + 0.0002\cos x)$; the results are illustrated in Figures 2–4.

For $l = 1 > l_0$, we take $\chi = 0.17 < \bar{\chi}, \tau = 1.8 < \tau_{00} = 2.09$, and the unique positive equilibrium $(u_*, v_*) = (0.2095, 0.4190)$ is stable (see Figure 2). Taking $\chi = 0.16 < \bar{\chi}, \tau = 2.095 > \tau_{00}$, we observe the spatially homogeneous periodic solution (see Figure 3). When $\chi > \bar{\chi}$, we take the concrete values of χ and τ as $P_3 - P_5$ of Figure 1(b), the spatially nonhomogeneous periodic solutions can appear near the Hopf bifurcation curve τ_{k0}. Moreover, there are various modes of periodic patterns when the values of χ are different (see Figure 4).

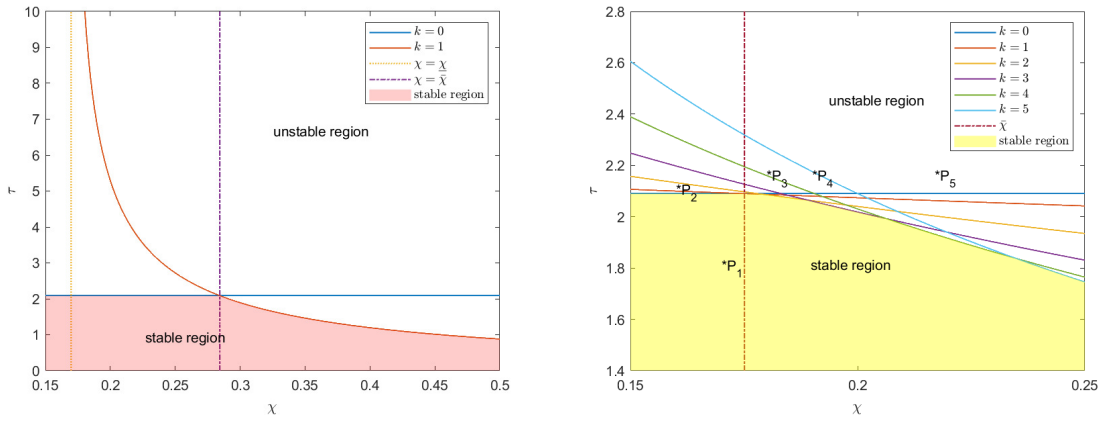

Figure 1. The bifurcation diagrams of system (1.3) in the $\chi - \tau$ plane with parameter chosen as in (3.1). (a) the Hopf bifurcation curves and stable region for $l = 0.1 < l_0$; (b) the Hopf bifurcation curves and stable region for $l = 1 > l_0$. The points P_1 $(0.17, 1.8)$, P_2 $(0.16, 2.095)$, P_3 $(0.18, 2.15)$, P_4 $(0.19, 2.15)$, *and* P_5 $(0.217, 2.15)$ marked in (b) are chosen for the numerical simulations.

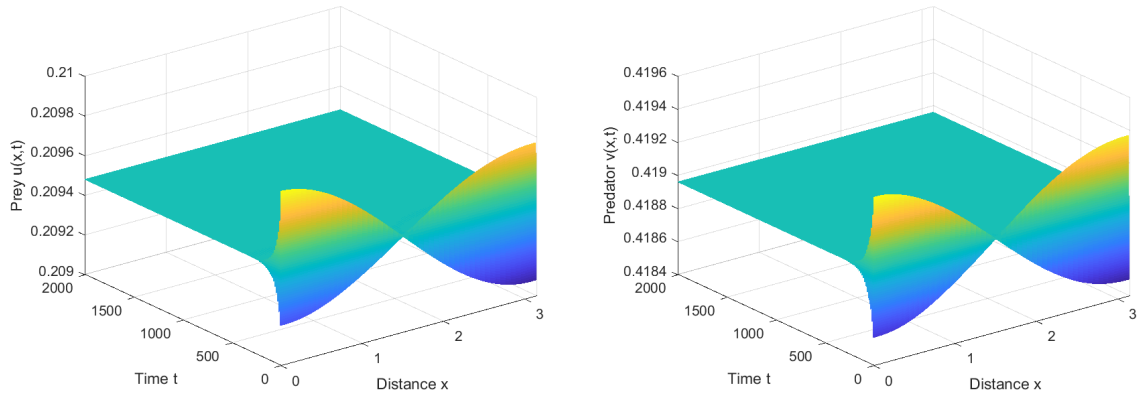

(a) **(b)**

Figure 2. Convergence to the positive equilibrium $(u_*, v_*) = (0.2095, 0.4190)$ of system (1.3) in the local stability region with parameters taken as (3.1) and $l = 1$ for P_1 (0.17, 1.8).

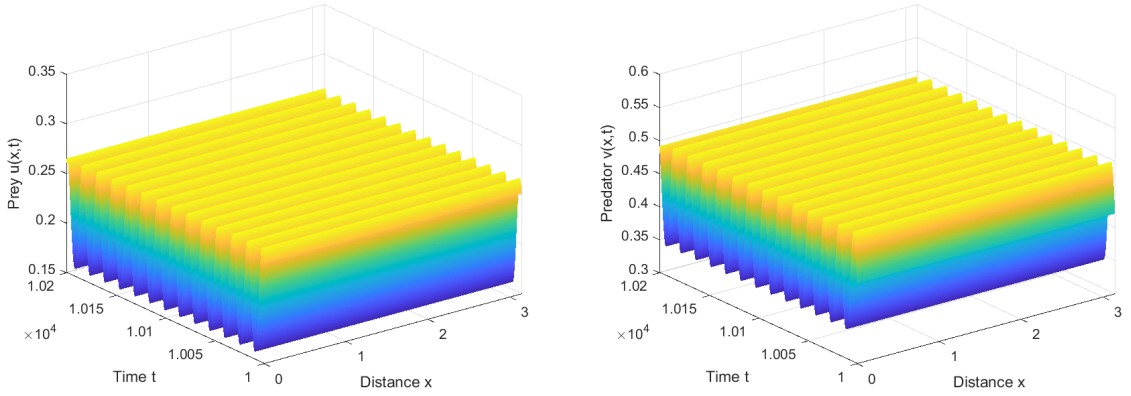

(a) **(b)**

Figure 3. The stability of the spatially homogeneous periodic solutions of (1.3) with parameters taken as (3.1) and $l = 1$ for P_2 (0.16, 2.095).

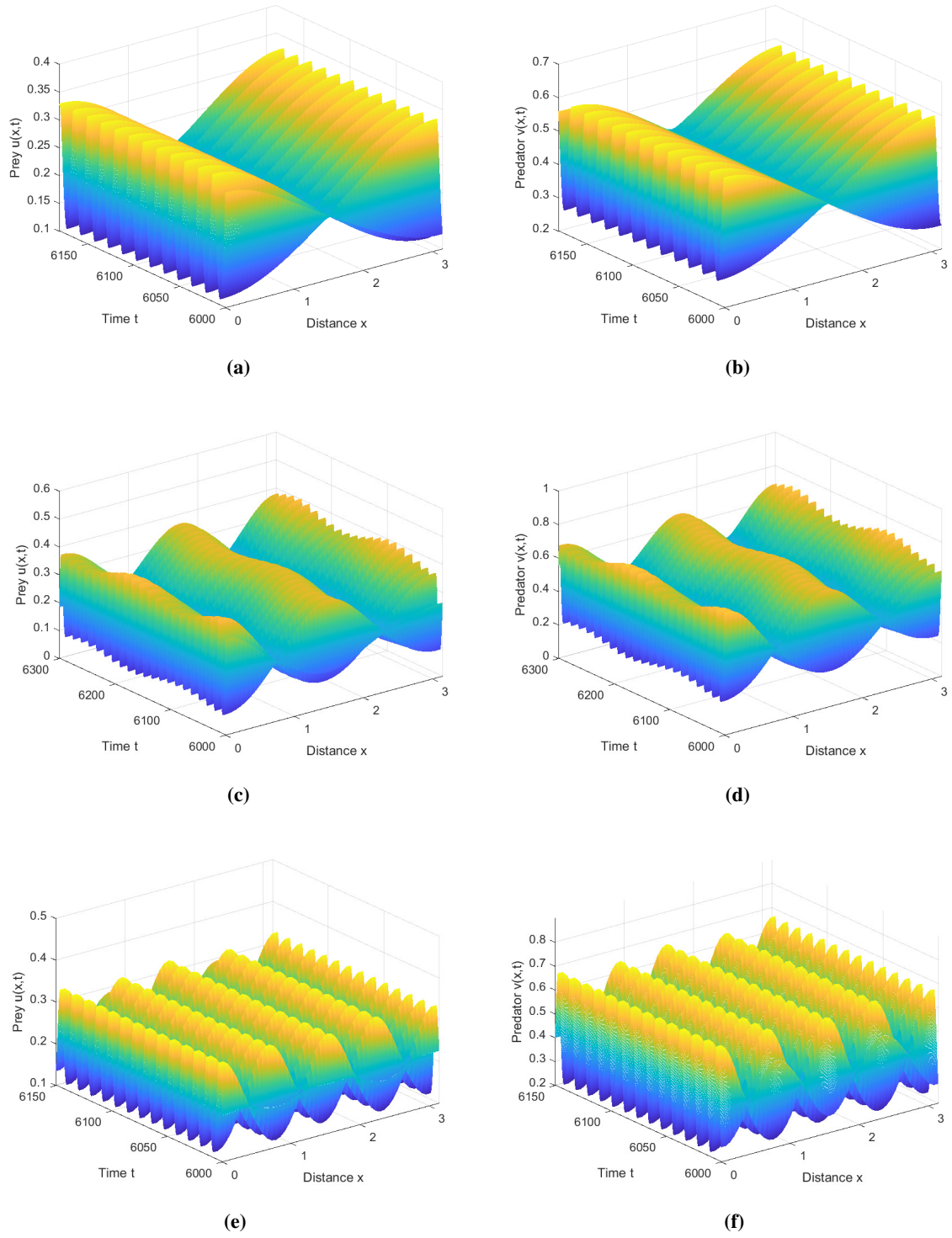

Figure 4. Numerical simulations of system (1.3) with the parameters as in (3.1) and $l = 1$. (a),(b)–(e),(f) illustrate the stability of the spatially nonhomogeneous periodic solutions for P_3 $(0.18, 2.15)$, P_4 $(0.19, 2.15)$, and P_5 $(0.217, 2.15)$, respectively, which have different modes.

3.2. *Case II* $\theta \geq \frac{\delta}{\beta r}$

By taking parameters as

$$d_1 = 0.1, d_2 = 0.2, r = 0.5, s = 0.5, \alpha = 1, \beta = 4, h = 0.3, v_p = 1, \tag{3.2}$$

we obtain $u_* = 0.6644, v_* = 0.3322, \delta = 0.0712, \theta = 0.6593 > \frac{\delta}{\beta r} = 0.0356$; by direct calculation, the conditions in Theorem 2.2 are satisfied. Let the domain size $l = 1$, then we calculate $\hat{\chi} = 15.2075$. From Theorem 2.2, the Hopf bifurcation curves can be drawn in the $\chi - \tau$ plane and the stability region is marked as shown in Figure 5. We find that Hopf bifurcation curves τ_{10} and τ_{30} intersect at point R_{13} (22.12, 6.687), which implies Hopf-Hopf bifurcation arising. Next, we choose two points P_6 (25, 2) and P_7 (22, 5) in Figure 5 to perform numerical simulations with the initial value $(u_0, v_0) = (u_* + 0.005 \cos x, v_* - 0.005 \cos x)$. For P_6 (25, 2) belonging to the stable region in Figure 5, Figure 6(a),(b) demonstrates the stability of (u_*, v_*). According to Theorem 2.2, the nonhomogeneous Hopf bifurcation will arise near the Hopf bifurcation curves τ_{k0} ($\underline{k} \leq k \leq K$) when $\chi > \hat{\chi}$, so the value of χ and τ taken in P_7 (22, 5) will induce spatially nonhomogeneous Hopf bifurcating periodic solutions, which have different modes (see Figure 6(c),(d)).

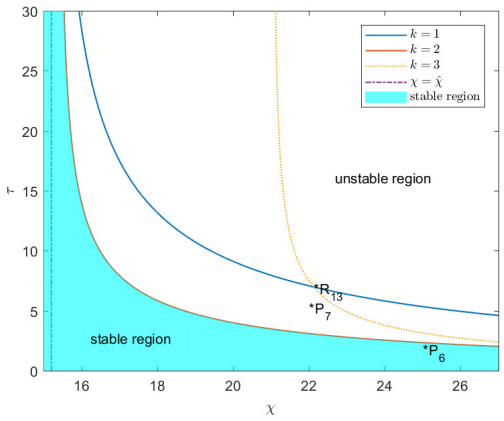

Figure 5. The stability region and Hopf bifurcation curves in the $\chi - \tau$ plane with the parameters are chosen as in (3.2). The points P_6 (25, 2) and P_7 (22, 5) are chosen for the numerical simulations.

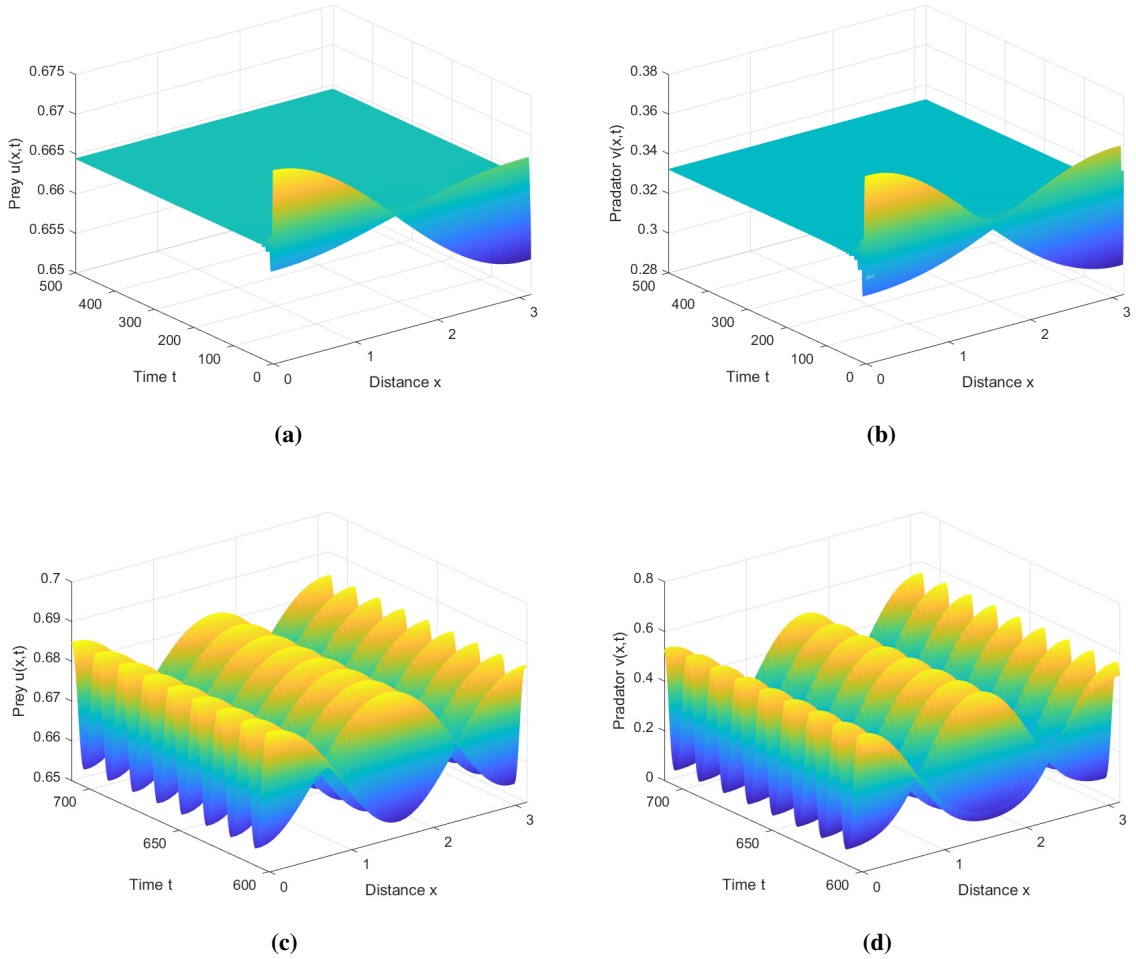

(a) **(b)**

(c) **(d)**

Figure 6. Numerical simulations of system (1.3) with the parameters as in (3.2) and $l = 1$. (a), (b) illustrate the stability of the unique positive equilibrium $(u_*, v_*) = (0.6644, 03322)$ for P_6 $(25, 2)$; (c), (d) illustrate the stability of the spatially nonhomogeneous periodic solutions for P_7 $(22, 5)$, which have different modes.

4. Conclusions

We explore a delayed diffusive prey-predator model with prey-taxis involving the volume-filling mechanism in this paper. Based on the taxis coefficient χ and time delay τ, we can classify system (1.3) into the following four cases: (i) $\chi = 0, \tau = 0$; (ii) $\chi > 0, \tau = 0$; (iii) $\chi = 0, \tau > 0$; (iv) $\chi > 0, \tau > 0$. Analyzing the stability and bifurcation, we obtained different pattern formations for different cases. For case (i), we know from [22] that the unique positive equilibrium (u_*, v_*) is locally asymptotically stable if $\theta \geq 0$, $0 < h < 1$. Hao et al. in [15] studied the case (ii), and suggested that the prey-taxis with the volume-filling mechanism will not induce Hopf bifurcation but the steady state bifurcation will arise. In the present paper, we explore the cases (iii) and (iv). Coincidentally the characteristic equation of the linear system of (1.3) for case (iii) is the same as that in [22] and the author found that Hopf bifurcation will occur due to the introduction of time delay, the periodic solutions at the first

critical value are spatially homogeneous, and Hopf-Hopf bifurcation will not arise. We mainly discuss case (iv) with the effect of prey-taxis with volume-filling mechanism and time delay, more complicated pattern formation that will appear, and how the results show that the system undergoes Hopf bifurction. Specifically, for $0 < \theta < \frac{\delta}{\beta r}$, the Hopf bifurcating periodic solutions near the first critical value of τ may be spatially homogeneous or nonhomogeneous with the different values of χ. When χ is larger than the critical value $\underline{\chi}$, the periodic patterns with different modes will arise for different values of χ. It can be proved that spatially homogeneous and nonhomogeneous bifurcation curves will intersect, which leads to Hopf-Hopf bifurcations. When $\theta \geq \frac{\delta}{\beta r}$, only spatially nonhomogeneous Hopf bifurcation will emerge. Moreover, we can observe from the numerical simulations that the nonhomogeneous Hopf bifurcation curves will intersect, which leads to the Hopf-Hopf bifurcation. The obtained results indicate that both prey-taxis and time delay play substantial roles in the pattern formation of prey-predator interactions, which may help with a deeper understanding of ecological systems.

Use of AI tools declaration

The authors declare they have not used Artificial Intelligence (AI) tools in the creation of this article.

Conflict of interest

The authors declare there is no conflict of interest.

References

1. A. J. Lotka, *Elements of Physical Biology*, Williams & Wilkins, Baltimore, 1925.
2. V. Volterra, Fluctuations in the abundance of a species considered mathematically, *Nature*, **119** (1927), 12–13. https://doi.org/10.1038/119012a0
3. H. Malchow, Spatio-temporal pattern formation in nonlinear non-equilibrium plankton dynamics, *Proc. R. Soc. B*, **251** (1993), 103–109. https://doi.org/10.1098/rspb.1993.0015
4. L. A. Segel, J. L. Jackson, Dissipative structure: an explanation and an ecological example, *J. Theor. Biol.*, **37** (1972), 545–559. https://doi.org/10.1016/0022-5193(72)90090-2
5. M. Banerjee, S. Petrovskii, Self-organised spatial patterns and chaos in a ratio-dependent predator–prey system, *Theor. Ecol.*, **4** (2011), 37–53. https://doi.org/10.1007/s12080-010-0073-1
6. M. Baurmann, T. Gross, U. Frudel, Instabilities in spatially extended predator–prey systems: spatio-temporal patterns in the neighborhood of Turing–Hopf bifurcations, *J. Theor. Biol.*, **245** (2007), 220–229. https://doi.org/10.1016/j.jtbi.2006.09.036
7. S. V. Petrovskii, H. Malchow, A minimal model of pattern formation in a prey-predator system, *Math. Comput. Modell.*, **29** (1999), 49–63. https://doi.org/10.1016/S0895-7177(99)00070-9
8. E. F. Keller, L. A. Segel, Initiation of slime mold aggregation viewed as an instability, *J. Theor. Biol.*, **26** (1970), 399–415. https://doi.org/10.1016/0022-5193(70)90092-5
9. E. F. Keller, L. A. Sege, Model for chemotaxis, *J. Theor. Biol.*, **30** (1971), 225–234. https://doi.org/10.1016/0022-5193(71)90050-6

10. T. Hillen, K. J. Painter, A user's guide to PDE models for chemotaxis, *J. Math. Biol.*, **58** (2009), 183–217. https://doi.org/10.1007/s00285-008-0201-3

11. N. Bellomo, A. Bellouquid, Y. Tao, M. Winkler, Toward a mathematical theory of Keller–Segel models of pattern formation in biological tissues, *Math. Models Methods Appl. Sci.*, **25** (2015), 1663–1763. https://doi.org/10.1142/S021820251550044X

12. K. J. Painter, Mathematical models for chemotaxis and their applications in self-organisation phenomena, *J. Theor. Biol.*, **481** (2019), 162–182. https://doi.org/10.1016/j.jtbi.2018.06.019

13. T. Hillen, K. J. Painter, Global existence for a parabolic chemotaxis model with prevention of overcrowding, *Adv. Appl. Math.*, **26** (2001), 280–301. https://doi.org/10.1006/aama.2001.0721

14. K. J. Painter, T. Hillen, Volume-filling and quorum-sensing in models for chemosensitive movement, *Can. Appl. Math. Q.*, **10** (2002), 501–543. Available from: http://www.math.ualberta.ca/ thillen/paper/CAMQ-final.pdf.

15. H. Hao, Y. Li, F. Zhang, Z. Lv, Bifurcation analysis of a predator-prey model with volume-filling mechanism, *Int. J. Wireless Mobile Comput.*, **25** (2023), 272–281. https://doi.org/10.1504/IJWMC.2023.134674

16. Y. Li, S. Li, J. Zhao, Global stability and Hopf bifurcation of a diffusive predator-prey model with hyperbolic mortality and prey harvesting, *Nonlinear Anal.-Model. Control*, **22** (2017), 646–661. https://doi.org/10.15388/NA.2017.5.5

17. M. Sambath, K. Balachandran, M. Suvinthra, Stability and Hopf bifurcation of a diffusive predator-prey model with hyperbolic mortality, *Complexity*, **21** (2016), 34–43. https://doi.org/10.1002/cplx.21708

18. Z. Zhang, R. K. Upadhyay, R. Agrawal, J. Datta, The gestation delay: a factor causing complex dynamics in Gause-type competition models, *Complexity*, **2018** (2018), 1–21. https://doi.org/10.1155/2018/1589310

19. S. A. Gourley, Y. Kuang, A stage structured predator-prey model and its dependence on maturation delay and death rate, *J. Math. Biol.*, **49** (2004), 188–200. https://doi.org/10.1007/s00285-004-0278-2

20. B. Barman, B. Ghosh, Dynamics of a spatially coupled model with delayed prey dispersal, *Int. J. Modell. Simul.*, **42** (2022), 400–414. https://doi.org/10.1080/02286203.2021.1926048

21. É. Diz-Pita, M. V. Otero-Espinar, Predator–prey models: a review of some recent advances, *Mathematics*, **9** (2021), 1783. https://doi.org/10.3390/math9151783

22. Y. Li, Dynamics of a delayed diffusive predator-prey model with hyperbolic mortality, *Nonlinear Dyn.*, **85** (2016), 2425–2436. https://doi.org/10.1007/s11071-016-2835-9

23. Q. Shi, Y. Song, Spatially nonhomogeneous periodic patterns in a delayed predator–prey model with predator-taxis diffusion, *Appl. Math. Lett.*, **131** (2022), 108062. https://doi.org/10.1016/j.aml.2022.108062

24. S. Chen, J. Shi, J. Wei, Global stability and Hopf bifurcation in a delayed diffusive Leslie–Gower predator–prey system, *Int. J. Bifurcation Chaos*, **22** (2012), 1250061. https://doi.org/10.1142/S0218127412500617

AIMS Press